Miniaturized polymer-coated FBGs for high-sensitivity biomedical pressure sensing

JPhys Photonics

Miniaturized polymer-coated FBGs for high-sensitivity biomedical pressure sensing

Journal of Physics: Photonics

OPEN ACCESS

RECEIVED
25 July 2025

REVISED
15 September 2025

ACCEPTED FOR PUBLICATION
28 September 2025

PUBLISHED
10 October 2025

PAPER

Miniaturized polymer-coated FBGs for high-sensitivity biomedical pressure sensing

Malhar A Nagar[1,3,*], **Giovanni Mingoia**[2,3], **Nadia Giovanna Boetti**[2] and **Davide Janner**[1,*]

[1] Dipartimento di Scienza Applicata e Tecnologia (DISAT), Politecnico di Torino, Turin, Italy
[2] Fondazione LINKS-Leading Innovation and Knowledge for Society, Turin, Italy
[3] These authors contributed equally to this work and share first authorship.
[*] Authors to whom any correspondence should be addressed.

E-mail: malhar.nagar@polito.it and davide.janner@polito.it

Keywords: bio-compatibility, elastomeric encapsulation, dynamic sensing, low-pressure detection, optical-fiber pressure sensors, real-time monitoring, static sensing

Supplementary material for this article is available online

Abstract

Continuous and real-time physiological pressure monitoring is essential for diagnosing and managing conditions such as intracranial hypertension, cardiovascular diseases, and gastrointestinal motility disorders. While fiber Bragg gratings (FBGs) offer several advantages over conventional electrical sensors, including immunity to electromagnetic interference and multiplexing capability for simultaneous multi-point sensing, their inherent low-pressure sensitivity limits their applicability in biomedical environments. This study investigates the enhancement of FBG pressure sensitivity through a polymer coating, such as polydimethylsiloxane (PDMS), is used to improve strain transfer and amplify the Bragg wavelength shift, with coating dimensions ($\sim$500 μm) compatible with pressure guidewires or catheters. A combined approach of finite element modeling and experimental validation demonstrated that, compared to uncoated sensors, PDMS-coated FBGs achieved up to 43-fold and 154-fold sensitivity enhancements for 500 μm and 800 μm coatings on 125 μm cladding fibers, and up to 212-fold and 339-fold improvements for corresponding coatings on 80 μm cladding FBGs. Under dynamic pressure, the sensors exhibited minimum detectable pressure amplitudes of 0.5 mmHg. These enhancements bring standard FBG sensors closer to real-time, minimally invasive continuous monitoring in pressure-guided catheters. Additionally, the mechanical robustness and multiplexing potential of coated FBGs enable non-invasive applications, such as smart walkers or wearable devices, broadening their utility across clinical and rehabilitative settings.

1. Introduction

The ability to measure physiological pressure with high sensitivity and stability is critical for various biomedical applications, including intracranial pressure (ICP) monitoring, vascular lesion assessment, and respiratory diagnostics [1]. Traditional pressure sensors, such as piezoresistive and electro-mechanical sensors, have been widely used in clinical settings but suffer from electromagnetic interference (EMI), signal drift, and limited stability. Optical fiber-based sensors, particularly fiber Bragg gratings (FBGs), offer an attractive alternative due to their compact size, inherent immunity to EMI, and, most importantly, their multiplexing capability, which enables a distributed approach with multiple sensing points along the same fiber. This, combined with their ability to monitor signals over time continuously, proves especially advantageous for tracking physiological parameters.

Recent advances in wearable photonics show that polymer optical fibers and FBGs can be embedded in wristbands and textiles for high-fidelity cardiorespiratory monitoring and even biometric identification, while remaining comfortable and robust under cyclic bending. Examples include a smart photonic wristband platform achieving simultaneous cardiorespiratory assessment and biometric identification [2], elastic 3D

printed material-packaged FBGs in chest/3D-printed housings that track respiration and heart rate [3], and broad reviews documenting polymer-encapsulated FBGs for body-worn sensing and catheter/guidewire integration [1].

However, bare FBGs have low-pressure sensitivity, typically in the range of 3.14–4.0 pm MPa^{-1} (0.42–0.5 fm $mmHg^{-1}$) [4, 5], which is largely insufficient for detecting subtle pressure variations in critical biomedical applications, such as monitoring ICPs (7–15 mmHg) or vascular pressures (∼80–120 mmHg) [6, 7]. By contrast, high-resolution manometry in the gastrointestinal tract (e.g. colonic manometry) generally involves pressure ranges of approximately 0–200 mmHg [8], which, while less stringent than intracranial or vascular parameters, still requires sufficiently sensitive sensing methods.

Several research groups have explored polymer-based solutions for FBG catheters and guidewires. For instance, Zhang *et al* packaged microstructured FBGs in a hyperelastic polymer for *in vivo* oesophageal pressure detection, achieving sensitivities on the order of 2.2 nm MPa^{-1} (i.e. 0.29 pm $mmHg^{-1}$), although requiring a 3 mm catheter diameter [9]. Arkwright *et al* employed flexible silicone diaphragm-based structures involving a rigid metallic substrate with an outer diameter (O.D.) of 3 mm [8] and biocompatible elastomeric sleeves with 2.2 mm O.D., which provided sensitivity of 1 pm $mmHg^{-1}$ [10] to track peristaltic movements in the esophagus and to diagnose disorders of colonic motility, respectively. Wang *et al* also employed silicone diaphragm-based structures involving coiled FBGs to track peristaltic movements in the gastrointestinal tract [11], again with an O.D. in the millimeter range. More recent work by Voigt *et al* and Becker demonstrated dual-layer and single-layer thermoplastic elastomeric coatings with different shore hardness, each exceeding 3 mm in O.D., with sensitivities of 0.7 $\mu\varepsilon$ $mbar^{-1}$ and 1.2 $\mu\varepsilon$ $mbar^{-1}$, suitable for high-resolution manometry [12, 13]. In a different investigation, Friedemann *et al* presented an integrated Fabry–Perot interferometer and an FBG-based pressure sensor for potentially monitoring real-time blood pressure and diagnosing conditions such as lumbar spinal stenosis with 2 mm O.D. and pressure sensitivity of 3 pm $mbar^{-1}$ [14].

While these approaches significantly increase FBG pressure sensitivity, the thick polymer layers employed impose constraints on miniaturization, often resulting in sensor diameters exceeding 2 mm. That limits their compatibility with smaller-scale guidewires and their application in minimally invasive biomedical procedures (e.g. blood vessels, brain, and heart monitoring). Conversely, device diameters as small as 200–400 μm have been reported with sensitivities of 7–20 times higher than bare FBGs [15, 16], employing, e.g, aggressively etched fibers with 25 μm cladding, which result in mechanically fragile sensors, which can be an issue for dynamic *in vivo* applications.

To address these limitations, we propose thin layers of polymer coatings to enhance strain transfer to the FBG in response to applied pressure. Elastomeric materials such as polydimethylsiloxane (PDMS) possess mechanical properties that are well suited for this purpose, including a low Young's modulus (∼870 kPa), a high Poisson's ratio (∼0.45), and biocompatibility. Importantly, PDMS exhibits minimal swelling in aqueous environments such as physiological saline or water [17, 18], with reported water uptake of only ∼0.05 wt% [19], and maintains mechanical stability over in aqueous environments for <3 d [20], well within the procedural timescales of typical biomedical applications, such as ∼40–45 mins in the case of assessment of vascular lesions(DEFINE FLAIR trials). By optimizing the polymer coating thickness, the fiber diameter, and mechanical compliance, significant improvements in pressure sensitivity can be achieved. This study aims to systematically investigate the effect of polymer coatings on the pressure sensitivity of FBGs using both theoretical and experimental approaches, with a particular focus on their potential integration into biomedical pressure sensing applications for minimally invasive procedures.

2. Theoretical modeling and simulations

FBG pressure sensing is based on the principle that an applied external pressure induces strain in the optical fiber, leading to a shift in the Bragg wavelength. The Bragg condition is given by:

$$\lambda_B = 2n_{eff}\Lambda, \tag{1}$$

where λ_B is the Bragg wavelength, n_{eff} is the effective refractive index of the fiber core, and Λ is the grating period. The change in Bragg wavelength due to applied strain can be expressed as:

$$\frac{\Delta\lambda_B}{\lambda_B} = [1 - p_e]\,\varepsilon_z, \tag{2}$$

where p_e is the effective strain-optic coefficient, and ϵ_z represents the axial strain. The axial strain, in turn, is influenced by the mechanical properties of the optical fiber and the surrounding polymer coating. For an

Table 1. Relevant mechanical and optical properties of the coating material (PDMS) and optical fiber.

Mechanical/optical properties	Material	
	Silica	PDMS
Refractive index	1.468	1.41
Density	2200 kg m^{-3}	976 kg m^{-3}
Young's modulus	72 GPa	870 kPa
Poisson's ratio	0.17	0.45
Yield strength	∼110–200 MPa	0.7–2.5 MPa
Elongation at break	2%–5%	100%–200%
Coefficient of thermal expansion	$\sim 0.55 \times 10^{-6}/°C$	$300\text{-}900 \times 10^{-6}/°C$

FBG with a polymer coating, the effective Young's modulus of the coated structure is modified according to equation (3) [9]:

$$E_{\text{eff}} = \frac{E_c.a_c + E_f.a_f}{a_{c+}\, a_f}, \tag{3}$$

where E_c and E_f are Young's moduli of the coating and fiber, respectively, and a_c and a_f are their corresponding cross-sectional areas. The polymer coating, with its lower modulus compared to the silica fiber (79.1 GPa), enhances strain transfer, resulting in a larger Bragg wavelength shift under the same applied pressure. Assuming isotropic radial stress and no shear stress, from Hooke's law, the axial strain can be expressed as:

$$\varepsilon_z = -\frac{(-2\nu)\,P}{E_{\text{eff}}}. \tag{4}$$

Substituting equations (3) and (4) in (2) the final pressure sensitivity formula reads:

$$\frac{\Delta\lambda_B}{P} = \frac{-(1-P_e)\,(-2\nu)}{E_{\text{eff}}}\lambda_B\,. \tag{5}$$

To predict performance and guide our design, we conducted a finite element analysis using ANSYS mechanical for static strain analysis. The model consisted of a 2D axisymmetric geometry representing a cross-section of the fiber (cladding diameters 125 μm and 80 μm) surrounded by a concentric cylinder of elastomeric polymer, with a variable coating diameter ranging from 200 μm to 1000 μm, as seen in figures S1 and S2. Appropriate material properties were assigned: silica for the optical fiber ($E_f = 73$ GPa, Poisson's ratio (ν_f) = 0.17) and PDMS-like polymer for the coating ($E_c = 870$ kPa, Poisson's ratio (ν_c) = 0.45. Table 1 presents some common mechanical and optical properties of the OF material (silica) and PDMS used in the simulations.

A uniform external radial pressure (1000 Pa, i.e. 7.5 mmHg) was applied to the outer boundary of the fiber/polymer, and axial strain in the fiber core was computed to estimate the Bragg wavelength shifts via the strain-optic coefficient. The results are reported in figure 1(a) and table 2, showing that merely reducing the bare fiber diameter from 125 μm to 80 μm has a negligible effect on sensitivity. However, coating a 125 μm fiber with a 500 μm-thick polymer resulted in a 50-fold increase in sensitivity, while an 80 μm fiber with the same coating diameter achieved a 128-fold improvement compared to its uncoated counterpart. Figure 1(b) illustrates that, increasing the coating diameters produces an increase in strain transfer to the fiber core. However, as seen in figure S2, for diameters above 650 μm, simulated pressure sensitivity values exceed theoretical predictions, likely due to non-uniform strain distributions and greater mechanical compliance.

Thinner fibers (80 μm) benefited more compared to 125 μm OF from increasing coating thicknesses, as illustrated by figures 1(a) and (b), due to the enhanced mechanical coupling. This is attributed to the increased compliance of the thinner fiber, which facilitates better mechanical coupling between the surrounding medium and the fiber core. However, due to the standard size of the catheters and pressure guide wires, ranging from 355.6 μm to 635 μm [6, 21, 22], the diameter of the coated material cannot be extended indefinitely. A 500 μm coating was therefore selected as an optimal balance, compatible with minimally invasive devices and also aligned with the resolution limits of the 3D-printed molds used for precise and repeatable FBG encapsulation at customized diameters.

For this coating diameter, the use of coatings with higher stiffness (i.e. increased elastic modulus) resulted in a reduction of the induced strain, as illustrated by figure 1(c). Conversely, higher values of Poisson's ratio were associated with enhanced strain transfer, as shown in figure 1(d). These findings collectively emphasize the necessity of carefully balancing parameters, such as fiber diameter, coating

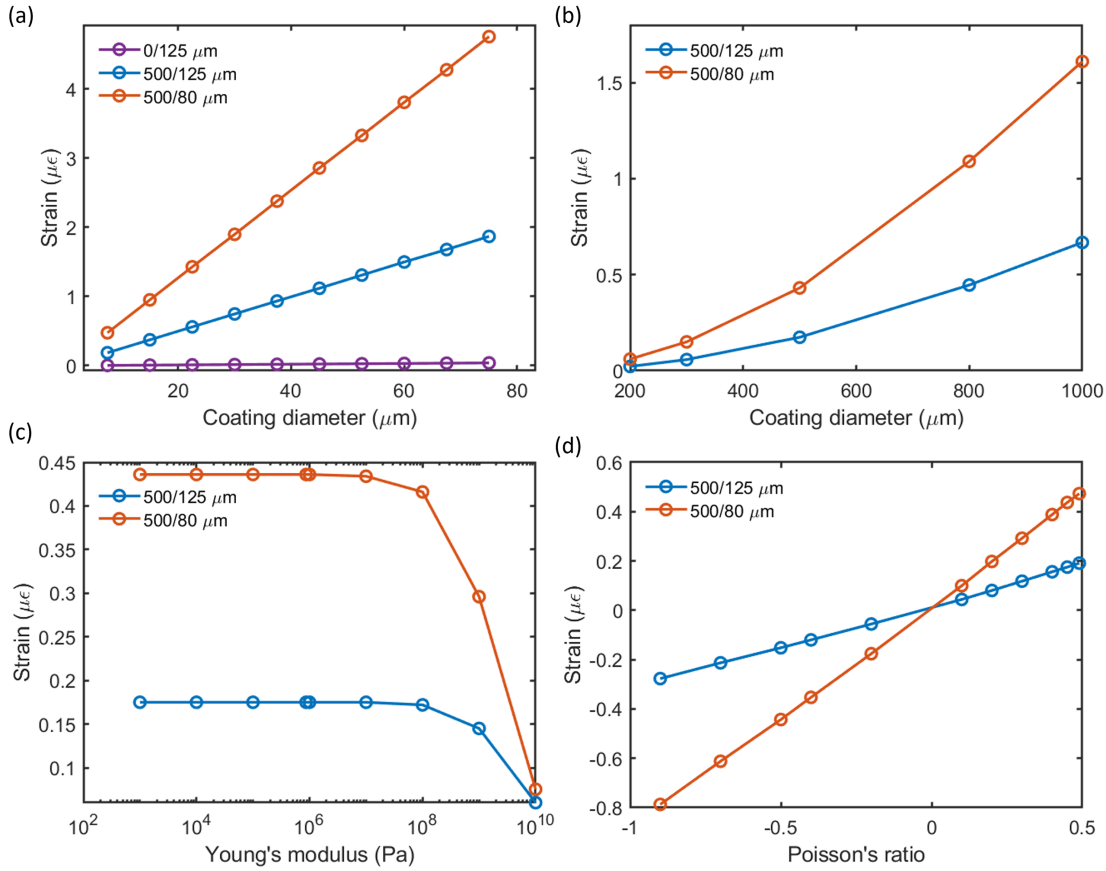

Figure 1. Finite element analysis of static strain response with 125 μm and 80 μm OF cladding diameters: (a) comparison of bare and 500 μm elastomer-coated optical fibers; (b) strain response with respect to the coating diameter; (c) effect of increasing Young's modulus on strain transfer ($\Phi = 500$ μm); (d) influence of Poisson's ratio on pressure-induced strain; under a fixed pressure of 7.5 mmHg.

Table 2. Enhancement of the sensitivity of bare and coated ($\Phi = 500$ μm) fiber for different fiber diameters.

	Sensitivity ($\mu\varepsilon$/mmHg)	
Optical fiber diameter (μm)	Bare	Coated
125	0.0005	0.025
80	0.0005	0.064

thickness, and polymer properties, particularly Young's modulus and Poisson's ratio, to optimize the sensitivity of fiber-optic pressure sensors.

3. Coating fabrication and experimental setup

Polymer coatings were applied to optical fibers through a custom injection molding process designed to achieve uniform thickness, robust fiber-polymer adhesion, and minimal surface defects. Although, the concept might look simple for coatings with diameters in the mm-size, producing coatings of sub-mm diameter with a good definition is a very delicate process. The multiple challenges to the process are related to the production of the molds, the casting of the polymer, and its curing and the management of the mechanical stress on the fiber that can accumulate during the curing.

In figure 2(a) we illustrate our proposed fabrication workflow. Although methods such as dip-coating, spin-coating, and spray-coating were initially considered, the high degree of thickness control, localized coating, and repeatability demanded by biomedical applications led us to develop customized 3D-printed molds using stereolithography b(SLA)-based 3D printing (Form3 3D printer) as seen in figures 2(a) and (b). Clear resin from Formlabs was identified as the most effective mold material due to its dimensional stability and smooth post-processing characteristics.

A multi-step surface treatment protocol was implemented to ensure reliable encapsulation. Two distinct surface-treatment protocols were evaluated to ensure uniform polymer coatings with strong fiber–polymer

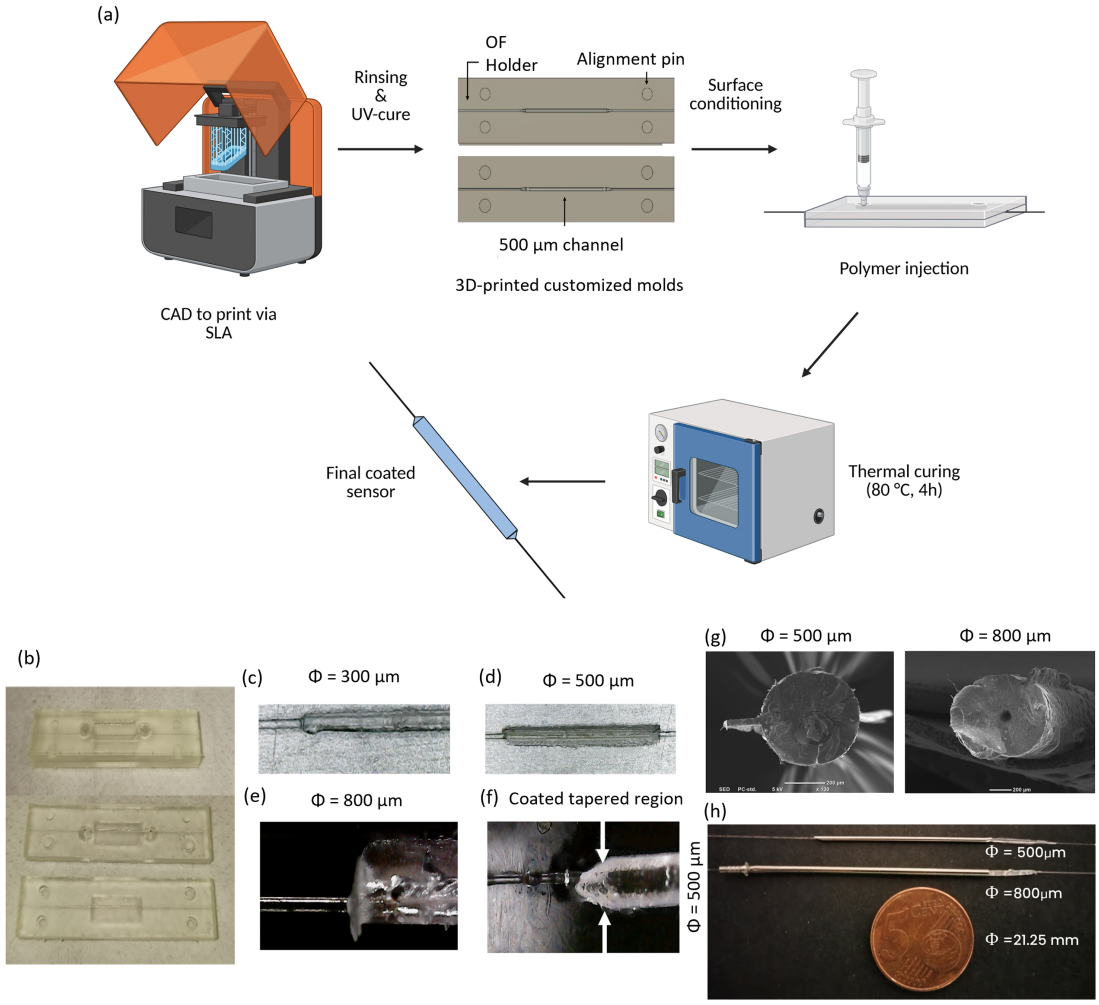

Figure 2. (a) Fabrication workflow of PDMS-coated FBG sensors using custom 3D-printed molds; (b) 3D printed mold for optical fiber coating; elastomeric coated FBGs of (c) 300 μm; (d) 500 μm; (e) 800 μm; and (f) demonstration of tapered region of 500 μm coating dimensions after surface treatments; (g) cross-sectional SEM images of FBGs with PDMS coatings of 500 μm and 800 μm outer diameters; (h) insertion of 500 μm and 800 μm PDMS-coated FBG sensor into catheter like enclosure with 600 μm and 1000 μm I.D. channels, respectively.

adhesion, while minimizing cure inhibition, which is an issue often encountered when using 3D printed parts as molds for silicone casting. In the first protocol, only the fiber underwent oxygen plasma exposure (0.5 mbar, 10 sccm, 100 W, 180 s) to remove contaminants and enhance bonding. Then, a mold release agent (Ease Release 200) was applied to the 3D-printed mold surfaces to prevent PDMS from adhering to residual monomers or oligomers, ensuring clean demolding. In the second protocol, both the mold and the fiber were exposed to the same oxygen plasma treatment, followed by chemical silanization of the mold using a 2% solution of 1H,1H,2H,2H-perfluorooctyltriethoxysilane (in ethanol). Beyond adjusting surface energy and improving polymer flow, this silane layer imparted a measurable degree of hydrophobicity to the mold, further minimizing interfacial adhesion between the cured PDMS and the mold walls, facilitating clean, damage-free demolding of the coated sensor.

For the encapsulation, Sylgard 184 elastomer and curing agent were mixed at a 10:1 ratio, thoroughly stirred, and degassed to remove entrapped air. The PDMS mixture was then injected slowly through an inlet in the mold containing the fiber until it rose through the opposite outlet. Subsequently, the mold was placed in an oven and heated to 80 °C for 4–5 h to achieve complete curing of the elastomer. Dimensional stability was maintained through precise mold fabrication channels (depending on the desired coating diameter) and curing protocols, collectively creating a controlled curing environment around the sensing region. This approach minimized interfacial voids and ensured strong adhesion between the fiber core and the polymer.

The excess polymer was removed in a secondary post-processing step using a nanosecond laser operated at 0.4 W, a 4 ns pulse width, and a 20 kHz repetition rate, scanned at a speed of 3 mm s^{-1}. A protective polyimide film was selectively applied to regions designated for removal; the laser then ablated the unwanted polymer without damaging the underlying fiber. This precise trimming step minimized dimensional

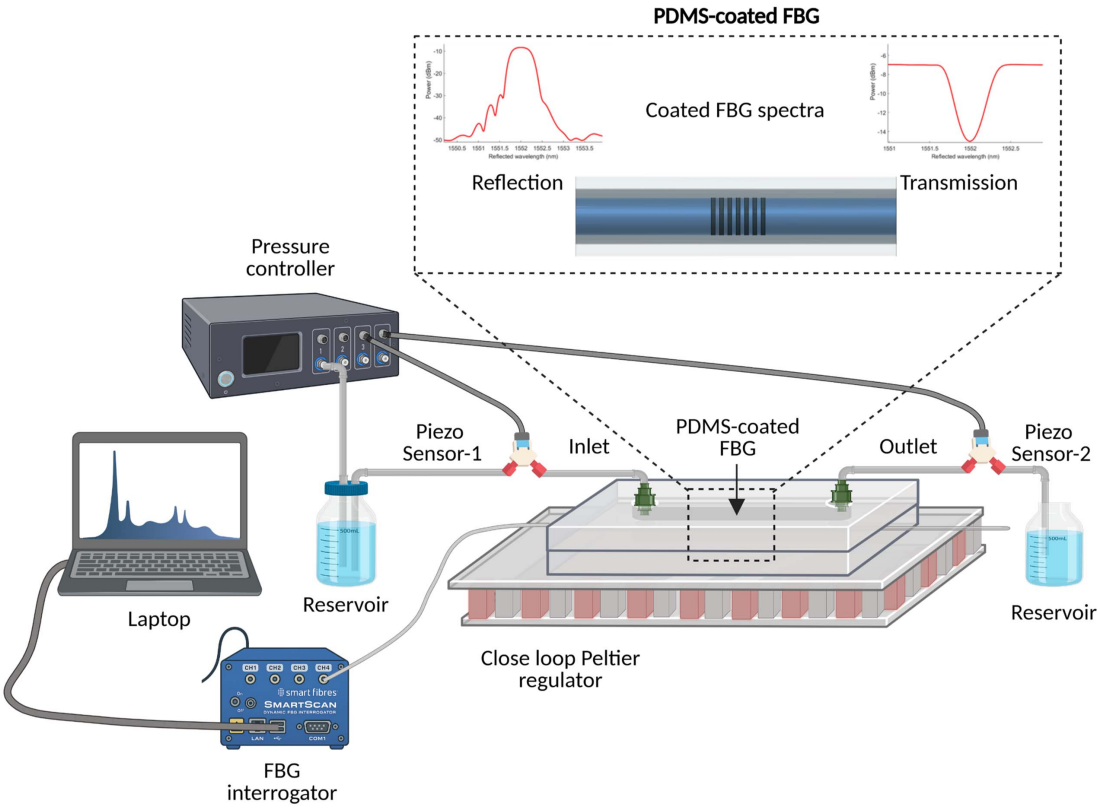

Figure 3. Experimental test bench for static and dynamic pressure sensing with a customized microfluidic channel and closed-loop temperature controller for coated optical sensor.

variations at the fiber's functional sensing region. Following extensive optimization, this approach consistently produced uniform coatings with diameters of 300 μm, 500 μm, and 800 μm, confirming the technique's versatility, as shown in figures 2(c)–(f). The corresponding cross-sectional morphology of the 500 μm and 800 μm PDMS-coated FBGs is shown in figure 2(g), with additional magnified optical microscopy and SEM images provided in figure S3, and the coating variability summarized in table S1. Neglecting the lateral protrusions, the coatings exhibited mean diameters of 487.8 μm ($\sigma = 12.7$ μm) and 806.7 μm ($\sigma = 11.9$ μm) for the 500 μm and 800 μm configurations, respectively. The uniform lateral protrusions observed in cross-section images (see figures 2(g) and S3(a–d)) arise from the two-part injection molding process using 3D-printed molds. The slight surface irregularities allow PDMS to seep between mold halves. Using the post-processing methods, these protrusions can be regularized, while the use of precision-machined aluminum or stainless-steel molds would further minimize such features at the cost of higher fabrication cost. Figure 2(h) demonstrates FBG sensors with 500 μm and 800 μm coating diameters inserted into 600 μm and 1 mm I.D. catheter-type channels, confirming their suitability for integration into compact, minimally invasive medical devices and miniaturized wearable sensors.

To experimentally validate the pressure sensitivity of the coated FBGs, a custom test bench was developed using a microfluidic pressure controller (OB1 Elveflow microfluidics) capable of delivering static pressures in the range of 0–1000 mbar (i.e. 0–750 mmHg). Figure 3 depicts the complete experimental setup. The uncoated and coated FBGs were embedded in a customized chip to detect fluid pressure (see figure S4). The pressure controller was connected to a de-ionized water reservoir, which supplied fluid to the microfluidic chip via polytetrafluoroethylene (PTFE) tubing at the inlet and outlet ports. To ensure accurate pressure delivery and maintain flow conditions, two piezoelectric pressure sensors (Elveflow microfluidics-MPS) were situated at each port end.

To estimate the local pressure at the FBG site, interpolation was performed by averaging the pressure readings at inlet and outlet ports to account for the pressure drop given by the resistance encountered by the flow. Indeed, due to pressure attenuation along the PTFE and silicone tubing, attributable to their length and internal diameter, the actual pressure measured at the FBG sensing location was reduced to approximately 0–450 mbar (0–338 mmHg). Figure S5 validates this approximation with further details. A secondary reservoir was placed downstream to collect the outflowing fluid.

A commercial interrogation unit (SmartScan) provided real-time measurements of the FBG reflection wavelengths. To mitigate temperature cross-sensitivity, the microfluidic chip was mounted on a Peltier element (ET-131-10-13-S, Adaptive Thermal Management) operated by a TEC-1091 controller (Meerstetter Engineering) with feedback from a PT-100 Class A RTD sensor (RS PRO, Ø1.5 mm, length 8 mm) embedded within the chip. The RTD provides an absolute accuracy of ±0.2 °C in the 25 °C–37 °C range with a response time of ∼0.4 s, while the controller regulates the Peltier with 0.005 °C resolution, yielding a stability of <±0.01 °C–0.02 °C around the setpoint. The Peltier module offers sufficient thermal headroom ($\Delta T_{max} = 74$ °C, $Q_{max} = 36.3$ W) to reject ambient fluctuations and maintain rapid compensation. As demonstrated in Fig. S6, the system maintained stable operation at 23.5 °C over 10 mins, confirming negligible residual drift. This ensured that the Bragg wavelength shifts observed in subsequent measurements originated predominantly from applied pressure rather than thermal fluctuations.

To assess the dynamic response characteristics of the polymer-coated FBG sensor, sinusoidal pressure waveforms with amplitudes ranging from 0–500 mbar (i.e. 0–375 mmHg) were applied at a frequency of 1 Hz using a programmable microfluidic pressure controller. Each pressure level was maintained for 30 s to allow the signal to stabilize and avoid transient settling effects. Notably, a reduction in the transmitted pressure amplitude was observed at the FBG sensor location, as indicated by the input and output pressure sensors (see figure S7). This fact, again, can be attributed to the compliant nature of the PTFE and silicone tubing, introducing energy loss at the pressure drive frequency.

4. Results and discussion

4.1. Baseline performance of bare FBGs

As an initial benchmark, bare FBGs were subjected to static pressures ranging from 0 to 750 mmHg, in 75 mmHg increments, over measurement intervals of >120 s per step. The reflected and transmitted spectra of the FBG under study, centered at 1552.06 nm with a 3 dB bandwidth of 0.50 nm, are presented in figures S8(a) and (b), respectively.

Initial measurements were acquired to establish stability and trend of Bragg wavelength shift with respect to pressure, however, significant drift in the Bragg wavelength emerged, with a standard deviation of 1.2 pm, corresponding to approximately 1 $\mu\varepsilon$, initially attributed to temperature cross-sensitivity, causing fluctuations comparable to or larger than the minor wavelength shifts induced by pressure, as seen in figure S9(a) and its corresponding sensitivity plot, figure S9(b). However, even under more stable temperature conditions using Peltier cell temperature controller, though providing relatively stable signal with standard deviation of <0.5 pm, the bare FBG did not display a meaningful correlation between external pressure and Bragg wavelength shift, confirming its inherently very poor pressure sensitivity (∼0.415 fm mmHg^{-1}), as shown in figures S9(c) and (d).

4.2. Enhanced static sensitivity with polymer coatings

To overcome the intrinsic limitations of the standard FBG, we applied polymer coatings and fabricated sensors with coated elastomeric layers of 500 μm and 800 μm, as detailed in the coating fabrication section. Additionally, another FBG sensor was incorporated to monitor temperature stability within a microfluidic chip over 120 s. Figures S10(a) and (b) represents the response of two FBGs for pressure and temperature measurements, respectively. The plots correspond to an input static pressure of 500 mbar (i.e., 375 mmHg) applied via a microfluidic pressure controller, resulting in a localized pressure of 210 mbar (i.e., 157 mmHg) at the center of the microfluidic chip position (i.e., location of embedded pressure sensing FBG). The FBGs recorded mean Bragg wavelengths of 1552.070 nm and 1561.763 nm, respectively, each exhibiting a standard deviation of 0.1 pm, indicating high measurement stability. This allowed for precise assessment of the microfluidic chip's internal conditions, ensuring reliable data acquisition for subsequent analyzes.

Figure 4(a) presents the pressure sensitivity plots for PDMS-coated FBGs with $\Phi = 500$ μm and $\Phi = 800$ μm coating diameters, under optimized conditions (relatively high uniformity in coating and temperature-controlled environment), observed over 60 s. The coated sensors displayed notable improvements of more than one and two orders of magnitude, respectively, in sensitivity over the uncoated FBG. The experimental results demonstrated a substantial enhancement in pressure sensitivity for PDMS-coated FBGs with 125 μm cladding. While bare FBGs exhibited a sensitivity of 3.14 pm MPa^{-1} (∼0.425 fm mmHg^{-1}), the coated FBGs achieved sensitivities of up to 135.59 pm MPa^{-1}(∼0.02 pm mmHg^{-1} with an $R^2 = 0.96$) and 482.14 pm MPa^{-1} (∼0.06 pm mmHg^{-1} with an $R^2 = 0.99$), representing a 43-fold and 154-fold increase in sensitivity. The sensitivity enhancement was dependent on coating thickness, with coatings of 500 μm and 800 μm providing the optimal balance between strain transfer and mechanical stability. The experimental results were also in close agreement with numerical simulations (as shown in table 3), which predicted pressure sensitivities of 208.80 pm MPa^{-1} (∼0.03 pm mmHg^{-1}) for

Table 3. Comparison of theoretical, simulated, and experimental pressure sensitivities observed for PDMS-coated ($\emptyset = 500\ \mu$m) FBG with a cladding diameter of 125 μm.

Coating diameter (μm)	Pressure sensitivity (fm/mmHg)		
	Theoretical	Simulation	Experimental
500	29.59	27.83	18.08
800	75.75	71.35	64.28

500 μm coating and 535.20 pm MPa^{-1} ($\sim$0.07 pm mmHg^{-1}) for 800 μm coating. The slight discrepancy between simulated and experimental values was attributed to slightly non-uniform cylindrical coating thickness, minor adhesion inconsistencies, and mechanical deformations during sensor fabrication.

Further enhancements in pressure sensitivity were achieved by reducing the FBG cladding diameter to 80 μm, leveraging the increased mechanical compliance and improved strain transfer associated with thinner fiber dimensions. The 500 μm PDMS-coated 80 μm FBG exhibited a pressure sensitivity of 665.79 pm MPa^{-1} ($\sim$0.09 pm mmHg^{-1} with an $R^2 = 0.99$), while the 800 μm coated sensor achieved a sensitivity of 1063.68 pm MPa^{-1} (0.14 pm mmHg^{-1} with an $R^2 = 0.99$), corresponding to approximately 212-fold and 339-fold improvements, respectively, compared to uncoated off-the shelf FBGs.

However, in the case of the 800 μm coating on the 80 μm cladding fiber, a non-linear pressure response was observed beyond 100 mbar (75 mmHg), as shown in figure S11. This non-linear saturation behavior arises from the combined effects of fiber-coating mechanics and the experimental configuration. The axial stiffness of a silica fiber scales with the product of its Young's modulus and the square of its radius (Er^2), thus, reducing the cladding diameter from 125 μm to 80 μm decreases stiffness by $\sim$59% and makes the thinner fiber significantly more compliant. When coupled with the lower modulus of PDMS ($\sim 10^6$ Pa) compared to silica ($\sim 10^{11}$ Pa) and the large 800 μm coating thickness, this creates a compliance mismatch of four to five orders of magnitude. Under these conditions, additional pressure beyond $\sim$75 mmHg could be increasingly absorbed by bulk compression of the PDMS rather than transferred to the fiber core, producing the observed saturation-like response. Additionally, at higher loads, the highly compliant geometry may also permit intermittent contact with the microfluidic chamber wall, introducing further mechanical constraints that reduce effective sensitivity. In practice, this configuration is thus best suited for low-pressure applications such as intracranial or bladder monitoring ($\leqslant$100 mmHg), where ultra-low detection thresholds are clinically valuable. For higher-pressure domains (e.g., arterial or gastrointestinal monitoring), more balanced designs such as the 500 μm coating on 80 μm fibers maintain both high sensitivity and a broader linear range. Potential strategies to further mitigate saturation include intermediate coating diameters ($\sim$600 μm), multiplexing hybrid sensor configurations on a single fiber, or applying non-linear calibration models to extend practical usability in the mid-pressure regime.

These findings highlight the critical need to optimize fiber diameter, coating thickness, and material properties to ensure both high sensitivity and linear performance across the target pressure range for biomedical sensing applications.

4.3. Dynamic sensitivity

The 500 μm coating thickness was selected for dynamic measurements as it provides an optimal balance between enhanced strain transfer and dimensional compatibility with standard catheter-based systems (typically 355–635 μm in diameter), making it well-suited for minimally invasive biomedical applications. To evaluate the dynamic response of elastomeric-coated FBGs with 125 μm and 80 μm cladding diameters, signal processing was performed using a custom MATLAB pipeline. The raw Bragg wavelength trace was first band-pass filtered using a 2nd-order Butterworth filter with a range of 0.1–3 Hz, centered around 1 Hz excitation frequency to remove unwanted frequency noise and drifts (see figures S12(a) and (b)). The power spectral density (PSD) was then computed using the Welch method, with a 40 s Hann window to achieve a frequency resolution of approximately 0.025 Hz. A comparison of a representative raw trace from FBG at an applied pressure amplitude of 32 mbar ($\sim$24 mmHg) with its filtered counterpart is reported in figures S13(a) and (b), and confirms that the filter removes the slow baseline wander while leaving the sinusoidal modulation intact.

Figure S14 compares the Welch PSDs of the filtered FBG traces for (a) 500 μm/125 μm (coating/cladding) and (b) 500 μm/80 μm (coating/cladding) optical fibers, respectively (with 50 dB offset), showing a distinct 1 Hz tone for various applied pressure amplitudes, 10–500 mbar (i.e., 7.5–375 mmHg) and corresponding amplitudes observed at the sensors' location, 0.6–40 mbar (i.e., 0.5–30 mmHg). From the PSD curve, the spectral power at 1 Hz, corresponding to the drive frequency, was extracted and converted to the decibel

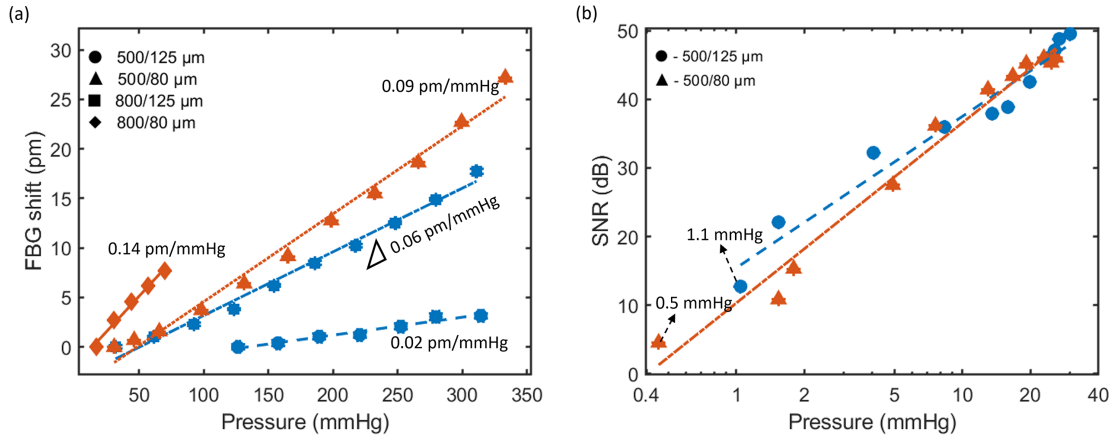

Figure 4. (a) Pressure sensitivity of coated FBGs under temperature-controlled conditions: 500 μm coating—0.02 pm mmHg^{-1} (125 μm FBG) and 0.09 pm mmHg^{-1} (80 μm FBG); 800 μm coating—0.06 pm mmHg^{-1} (125 μm FBG) and 0.14 pm mmHg^{-1} (80 μm FBG); (b) Dynamic pressure sensitivity plots for 500 μm/125 μm (coating/cladding) and 500 μm/80 μm (coating/cladding) optical fibers.

scale. The signal-to-noise ratio (SNR) was calculated by comparing the 1 Hz PSD value with the average PSD from nearby non-harmonic frequency bands and plotted as a function of the applied pressure amplitude.

The relationship between SNR and pressure amplitude, as illustrated in figure 4(b), exhibited a non-linear trend for both 125 μm and 80 μm cladding FBGs with 500 μm PDMS coatings. To better capture this behavior, a logarithmic fitting approach was applied, yielding a strong correlation for both configurations. For the 125 μm cladding fiber, the SNR response followed the equation SNR = 9.58 $\log(x)$ + 15.43, with an R^2 of 0.96. The 80 μm cladding FBG exhibited an enhanced logarithmic response, described by SNR = 11.39 $\log(x)$ + 10.32, with an R^2 of 0.983. Notably, the elastomeric-coated FBG sensors demonstrated the capability to resolve minimum pressure amplitude changes of approximately 1.39 mbar (∼1.04 mmHg) for the 125 μm cladding configuration and 0.61 mbar (∼0.46 mmHg) for the 80 μm cladding, as shown in figures 4(b) and S14(a) and (b), underscoring their low detection threshold and suitability for sensing subtle pressure fluctuations in the low-frequency physiological pressure range.

While the coated sensors demonstrated excellent pressure sensitivity, *in-vivo* environments are not perfectly stable, and polymer coatings may alter thermal response compared to bare silica fibers. To assess this, we quantified thermal stability over 900 s under non-temperature-controlled conditions. At zero applied pressure, the bare FBG showed σ = 1.22 pm compared to σ = 1.40 pm for the 500 μm/125 μm coated sensor (see figures S15(a) and (c)), while under 300 mmHg the corresponding values were σ = 0.40 pm and σ = 0.96 pm (see figures S15(b) and (d)). This modest increase in standard deviation compared to those observed for bare FBGs under non-temperature-contolled conditions, reflects the effect of higher coefficient of thermal expansion of PDMS (300–900 × 10^{-6}/ °C) relative to silica (∼0.55 × 10^{-6}/ °C) [1]. Interestingly, whereas bare FBGs showed no correlation between applied pressure and Bragg shift, under both uncontrolled and stabilized thermal conditions (see figure S9), the coated FBG exhibited an apparent correlation with sensitivity of 0.046 pm mmHg^{-1} with R^2 of 0.66 (see figure S16). This, however, is partly an artefact of thermal cross-talk, which artificially inflated sensitivity and reduced accuracy. Under stabilized temperature control, the same sensor showed a much lower apparent cross-talk of 0.020 pm mmHg^{-1} with R^2 = 0.96 (see figure 4(a)), confirming that thermal effects were the source of the deviation. Importantly, in dynamic conditions relevant to physiology, temperature fluctuations are inherently slow, and generally limited to $\leqslant$1 °C across time scales ranging from minutes (5–10 min) to hours or a full day [23–25], while pressure oscillations occur at 1–2 Hz. To replicate this, we applied a 1 Hz sinusoidal pressure with amplitude of ∼15 mmHg superimposed on either a +0.5 °C ramp over 120 s and an open-loop drift of ∼0.4 °C over 10 min. In both cases, pressure oscillations remained distinct and were cleanly recovered by bandpass filtering (see figures S17 and S18 respectively), demonstrating that physiologic-band pressure dynamics can be robustly isolated from slower thermal drifts.

Additionally, mechanical robustness was verified by repeatedly inserting the coated FBGs into catheter-like channels (600 μm and 1 mm ID) and subjecting them to bending (figure S19). Subsequent static and dynamic measurements showed results consistent with the unbent condition, confirming that the PDMS-coated sensors withstand realistic handling and insertion stresses without loss of performance. These static and dynamic pressure sensing results confirm the sensor's ability to resolve static and periodic pressure

variations in the low-frequency physiological band, validating its potential applicability for biomedical pressure sensing for minimally invasive and non-invasive platforms.

A major advantage of FBGs lies in their intrinsic multiplexing capability, enabling multi-point sensing along a single fiber for minimally invasive pressure mapping. The localized coating approach presented here is inherently scalable, either through multi-cavity mold designs that allow simultaneous coating of multiple gratings, or through sequential localized coating strategies depending on the desired sensor array configuration. For such multiplexed systems, mechanical cross-talk is governed by strain-transfer physics. The shear-lag models predict an exponential decay of transferred strain away from the coated region, with a finite influence length determined by coating thickness, modulus, and fiber geometry [26]. To avoid overlap of these influence zones, prior studies of polymer-embedded FBG arrays have demonstrated that a center-to-center separation of 5–10 mm is sufficient to ensure independent responses [8, 27]. Based on this evidence, a conservative minimum spacing of $\geqslant$5 mm between coated FBGs can be recommended for pressure mapping applications.

Future work will focus on systematically optimizing coating length and inter-sensor spacing to balance sensitivity with spatial resolution in multiplexed arrays, as well as evaluating long-term stability of PDMS-coated FBGs under prolonged immersion in physiological buffers. Sterilization compatibility will also be addressed, with emphasis on alternatives to autoclaving or gamma irradiation, such as ethylene oxide, hydrogen peroxide plasma, or UV treatment that are more suitable for preserving PDMS properties [28, 29]. While the coated sensors are intended to be embedded within catheter or guidewire sheaths where biofouling is less critical, surface modification strategies such as PDMS-PEG copolymer blending could be explored for future direct-contact applications [30]. These studies will be critical for translating the sensors toward clinically deployable applications.

5. Conclusion

This study demonstrates that miniaturized PDMS-coated FBG sensors provide substantial enhancement in both static and dynamic pressure sensitivity, establishing their suitability for a wide range of biomedical pressure sensing applications. For 125 μm-diameter fibers, optimizing the polymer coating thickness to 500 μm and 800 μm improved pressure sensitivity by 43 times and 154 times, respectively, compared to standard FBGs. Further improvements of 212 and 339 times, respectively, were achieved for 80 μm diameter fibers, reaching a maximum sensitivity of 0.14 pm mmHg^{-1}, which is a suitable value for detecting clinical signals.

These improvements were consistently validated through analytical modeling, finite element simulations, and experimental measurements. Furthermore, the coated sensors exhibited robust dynamic responses with sensitivities enabling minimum detectable pressure amplitudes down to 0.5 mmHg for the 80 μm cladding, highlighting their capability to resolve ultra-low pressure fluctuations with strong signal-to-noise performance.

The integration of these sensors into biomedical platforms presents significant potential for real-time, multi-point physiological pressure monitoring, offering a scalable and cost-effective alternative to existing optical pressure sensors. Their compact form factor and enhanced sensitivity make them particularly suitable for minimally invasive devices, as well as for integration into smart textiles, wearable technologies, and rehabilitative monitoring systems.

Data availability statement

The data that support the findings of this study are openly available at the following URL/DOI: 10.5281/zenodo.16413673 [31].

Acknowledgments

This research was funded by the European Union's Horizon 2020 research and innovation programme under the Marie Sklodowska-Curie Grant Agreement No. 860185, as part of the PHAST-ITN project. This study was also supported within the BIOPHET project—funded by European Union—Next Generation EU within the PRIN 2022 PNRR program (D.D.1409 del 14/09/2022 Ministero dell'Università e della Ricerca).

Author contributions

Malhar A Nagar 0009-0006-7386-3538
Conceptualization (lead), Data curation (lead), Formal analysis (lead), Funding acquisition (supporting), Investigation (lead), Methodology (lead), Project administration (equal), Resources (supporting), Software (lead), Supervision (supporting), Validation (lead), Visualization (equal), Writing – original draft (lead), Writing – review & editing (equal)

Giovanni Mingoia 0009-0007-3035-1986
Conceptualization (supporting), Data curation (equal), Formal analysis (supporting), Funding acquisition (supporting), Investigation (equal), Methodology (equal), Project administration (supporting), Resources (supporting), Software (supporting), Supervision (supporting), Validation (equal), Visualization (equal), Writing – original draft (supporting), Writing – review & editing (equal)

Nadia Giovanna Boetti 0000-0002-5269-2390
Funding acquisition (equal), Project administration (equal), Resources (equal), Writing – review & editing (supporting)

Davide Janner 0000-0001-7954-979X
Conceptualization (equal), Funding acquisition (lead), Project administration (lead), Resources (equal), Writing – original draft (equal), Writing – review & editing (lead)

References

[1] Nagar M A and Janner D 2024 Polymer-based optical guided-wave biomedical sensing: from principles to applications *Photonics* **11** 10
[2] Li W *et al* 2025 Wearable photonic smart wristband for cardiorespiratory function assessment and biometric identification *Opto-Electron. Adv.* **8** 240254–21
[3] Tavares C, Leitão C, Lo Presti D, Domingues M F, Alberto N, Silva H and Antunes P 2022 Respiratory and heart rate monitoring using an FBG 3D-printed wearable system *Biomed. Opt. Express* **13** 2299–311
[4] Xu M G, Reekie L, Chow Y T and Dakin J P 1993 Optical in-fibre grating high pressure sensor *Electron. Lett.* **29** 398–9
[5] Schenato L, Rong Q, Shao Z, Quiao X, Pasuto A, Galtarossa A and Palmieri L 2025 Highly sensitive FBG pressure sensor based on a 3D-printed transducer *IEEE Journals & Magazine | IEEE Xplore* (available at: https://ieeexplore.ieee.org/document/8726115) (Accessed 08 Febuary 2025)
[6] Correia R, James S, Lee S-W, Morgan S P and Korposh S 2018 Biomedical application of optical fibre sensors *J. Opt.* **20** 073003
[7] Tosi D, Poeggel S, Iordachita I and Schena E 2018 11—fiber optic sensors for biomedical applications *Opto-Mechanical Fiber Optic Sensors* ed H Alemohammad (Butterworth-Heinemann) pp 301–33
[8] Arkwright J W, Blenman N G, Underhill I D, Maunder S A, Szczesniak M M, Dinning P G and Cook I J 2009 *In-vivo* demonstration of a high resolution optical fiber manometry catheter for diagnosis of gastrointestinal motility disorders *Opt. Express* **17** 4500–8
[9] Zhang W, Ni X, Wang J, Ai F, Luo Y, Yan Z, Liu D and Sun Q 2019 Microstructured optical fiber based distributed sensor for *in vivo* pressure detection *J. Lightwave Technol.* **37** 1865–72
[10] Arkwright J W, Underhill I D, Maunder S A, Blenman N, Szczesniak M M, Wiklendt L, Cook I J, Lubowski D Z and Dinning P G 2009 Design of a high-sensor count fibre optic manometry catheter for in-vivo colonic diagnostics *Opt. Express* **17** 22423–31
[11] Wang D H-C, Abbott A, Maunder S A, Blenman N G and Arkwright J W 2012 A miniature fiber Bragg grating pressure sensor for in-vivo sensing applications *Proc. SPIE* **8421** 656–9
[12] Voigt S *et al* 2010 Homogeneous catheter for esophagus high-resolution manometry using fiber Bragg gratings *Proc. SPIE* **7559** 61–70
[13] Becker M *et al* 2012 Characterization of fiber Bragg grating-based sensor array for high resolution manometry *Proc. SPIE* **8439** 15–23
[14] Friedemann M, Voigt S and Mehner J 2022 Pressure sensor catheter based on fiber tip Fabry-Pérot-interferometer and fiber Bragg grating for temperature compensation: fiber-optic hybrid sensor catheter for invasive pressure measuring *Curr. Direct. Biomed. Eng.* **8** 404–7
[15] Dennison C R and Wild P M 2008 Enhanced sensitivity of an in-fibre Bragg grating pressure sensor achieved through fibre diameter reduction *Meas. Sci. Technol.* **19** 125301
[16] Dennison C R, Wild P M, Wilson D R and Cripton P A 2008 A minimally invasive in-fiber Bragg grating sensor for intervertebral disc pressure measurements *Meas. Sci. Technol.* **19** 085201
[17] Lee J N, Park C and Whitesides G M 2003 solvent compatibility of poly(dimethylsiloxane)-based microfluidic devices *Anal. Chem.* **75** 6544–54
[18] Zuo C, Xu S, Ding X, Jin W, Xing W and Ke X 2022 Transmission of sodium chloride in PDMS membrane during pervaporation based on polymer relaxation *J. Membr. Sci.* **659** 120812
[19] Wong W S Y, Hauer L, Naga A, Kaltbeitzel A, Baumli P, Berger R, D'Acunzi M, Vollmer D and Butt H-J 2020 Adaptive wetting of polydimethylsiloxane *Langmuir* **36** 7236–45
[20] Zhang Y, Adam C, Rehnstrom H and Contera S 2024 Temporal evolution of mechanical properties in PDMS: a comparative study of elastic modulus and relaxation time for storage in air and aqueous environment *J. Mech. Behav. Biomed. Mater.* **160** 106779
[21] Ulacia P, Rimac G, Lalancette S, Belleville C, Mongrain R, Plante S, Rusza Z, Matsuo H and Bertrand O F 2022 A novel fiber-optic based 0.014″ pressure wire: designs of the OptoWire™, development phases, and the O first-in-man results *Catheter. Cardiovasc. Interv.* **99** 59–67

[22] Morton Kern M D 2016 Chief of medicine, and P of Mof M. associate chief cardiology, 'comparing FFR tools: new wires and a pressure microcatheter', *Cath Lab Digest* vol 24 p 5 (available at: www.hmpgloballearningnetwork.com/site/cathlab/article/comparing-ffr-tools-new-wires-pressure-microcatheter)
[23] Mrozek S, Vardon F and Geeraerts T 2012 Brain temperature: physiology and pathophysiology after brain injury *Anesthesiol. Res. Pract.* **2012** 989487
[24] Saad H and Aladawy M 2013 Temperature management in cardiac surgery *Glob. Cardiol. Sci. Pract.* **2013** 44–62
[25] Stefanadis C, Toutouzas K, Tsiamis E, Mitropoulos I, Tsioufis C, Kallikazaros I, Pitsavos C and Toutouzas P 2003 Thermal heterogeneity in stable human coronary atherosclerotic plaques is underestimated *in vivo*: the "cooling effect" of blood flow *J. Am. Coll. Cardiol.* **41** 403–8
[26] Falcetelli F, Rossi L, Di Sante R and Bolognini G 2020 Strain transfer in surface-bonded optical fiber sensors *Sensors* **20** 3100
[27] Kanellos G T, Papaioannou G, Tsiokos D, Mitrogiannis C, Nianios G and Pleros N 2010 Two dimensional polymer-embedded quasi-distributed FBG pressure sensor for biomedical applications *Opt. Express* **18** 179–86
[28] Bathina M N, Mickelsen S, Brooks C, Jaramillo J, Hepton T and Kusumoto F M 1998 Safety and efficacy of hydrogen peroxide plasma sterilization for repeated use of electrophysiology catheters *J. Am. Coll. Cardiol.* **32** 1384–8
[29] Greaney A J, McCarthy C M, Vethil J P, Abubaker M, Reardon E C, Crowley F D, Cunnane E M and Mulvihill J J E 2025 A comprehensive protocol for PDMS fabrication for use in cell culture *PLoS One* **20** e0323283
[30] Gökaltun A, Kang Y B, Yarmush M L, Usta O B and Asatekin A 2019 Simple surface modification of poly(dimethylsiloxane) via surface segregating smart polymers for biomicrofluidics *Sci. Rep.* **9** 7377
[31] Nagar M A 2025 Miniaturized Polymer-Coated FBGs for High Sensitivity Biomedical Pressure Sensing *Zenodo* (https://doi.org/10.5281/zenodo.16413673)